ELSEVIER

Journal of Chromatography A, 918 (2001) 361–370

JOURNAL OF CHROMATOGRAPHY A

www.elsevier.com/locate/chroma

Different elution modes and field programming in gravitational field-flow fractionation
III. Field programming by flow-rate gradient generated by a programmable pump

Jana Plocková*, Josef Chmelík

Institute of Analytical Chemistry, AS CR, 611 42 Brno, Czech Republic

Received 24 July 2000; received in revised form 23 February 2001; accepted 23 February 2001

Abstract

Gravitational field-flow fractionation (GFFF) utilizes the Earth's gravitational field as an external force that causes the settlement of particles towards the channel accumulation wall. Hydrodynamic lift forces oppose this action by elevating particles away from the channel accumulation wall. These two counteracting forces enable modulation of the resulting force field acting on particles in GFFF. In this work, force-field programming based on modulating the magnitude of hydrodynamic lift forces was implemented via changes of flow-rate, which was accomplished by a programmable pump. Several flow-rate gradients (step gradients, linear gradients, parabolic, and combined gradients) were tested and evaluated as tools for optimization of the separation of a silica gel particle mixture. The influence of increasing amount of sample injected on the peak resolution under flow-rate gradient conditions was also investigated. This is the first time that flow-rate gradients have been implemented for programming of the resulting force field acting on particles in GFFF.

Keywords: Field-flow fractionation; Field programming; Flow-rate gradients; Hydrodynamic lift forces

1. Introduction

The separation effect in field-flow fractionation (FFF) is accomplished by the combined action of a non-uniform flow velocity profile of a carrier liquid and an applied transverse force field [1]. Gravitational field-flow fractionation (GFFF) is experimentally the simplest and cheapest among the family of FFF techniques [2]. It utilizes the Earth's gravitational field as the external force field that causes settlement of particles towards the channel accumulation wall. However, there are other forces acting on the particles during the separation process: hydrodynamic lift forces (HLF) [3] and electrostatic interactions [4].

GFFF has been successfully applied to a wide variety of inorganic, synthetic and biological particulate materials. It has been employed for the separation, characterisation and micropreparation of cells [5,6], starch granules [7], silica gel particles [4,8–10], polymer latexes [11,12], fine coal particles and residues from coal liquefaction [13].

In many FFF techniques, force-field programming

*Corresponding author.

E-mail address: janap@iach.cz (J. Plocková).

0021-9673/01/$ – see front matter
PII: S0021-9673(01)00706-3

has been implemented in order to broaden the versatility and to optimize separations in terms of time, resolution and detection limit [14–17]. Due to the constant and relatively weak gravitational field, it seems that the applicability of force-field programming in GFFF is rather limited. However, as suggested and justified in previous work [18,19], there are several possibilities to control the resulting force field acting on particles in GFFF. In focusing (hyperlayer) elution mode, at least two counteracting forces determine the retention ratio of particles [20,21]. In GFFF, these counteracting forces are the gravitational force on one hand and hydrodynamic lift forces [3] (or in some cases electrostatic repulsion [4]) on the other. HLF [22] tend to drive the particles away from the channel accumulation wall and to focus them into narrow zones. In the flow velocity profile, these zones are located at those positions where the resulting force acting on the particles is zero, i.e. where the effective particle weight equals the HLF. It follows that any change in these counteracting forces results in a change of the retention ratio. Thus, we can control the retention of particles by modulation of HLF action [18].

Several attempts have been made to describe HLF action by a mathematical equation. All the equations include the dependence of the HLF magnitude on the flow-rate. According to Refs. [23–25], the magnitude of the inertial lift force is proportional to the square of the average linear velocity. Ref. [26] focused on the near-wall lift force, and the linear dependence on the average linear velocity was empirically obtained for particles travelling near the channel wall. According to all these equations, the magnitude of the HLF increases with increasing flow-rate. It follows that we can modulate the HLF action and thus the resulting force field acting on particles by changing the flow-rate. There are two possibilities to achieve these changes: by programmed pumping or with channels of non-constant cross-sections [18].

The dependence of the retention ratio on the flow-rate in focusing elution mode in GFFF has been widely studied experimentally [4,8,9,19]. The size-based retention order of analytes in focusing elution mode is reversed compared to Brownian elution mode [3,8,9]. According to Refs. [23–25], the inertial HLF increases with the fourth power of the particle radius, while the counteracting effective particle weight is proportional to the third power of the particle radius. It follows that, with increasing particle radius, the predominance of HLF proportionally increases, thus the larger particles elute first [9,19].

In this work, different types of flow-rate gradient, ranging as shown in the previous work [19], were implemented in the separation of a model silica gel particle mixture and tested as tools for optimization of the separation. We aimed to reduce the total duration of the separation without any loss or even with an increase of peak resolution compared to experiments at constant flow-rates. The flow-rate programming described in this work differs from that published by Giddings et al. [27] in sedimentation FFF. Whereas programming of the rotation speed and carrier liquid density introduced by Yang et al. [28] are examples of force-field programming, no force-field programming occurred in Ref. [27]. No increase of the retention ratio with increasing flow-rate was observed during those velocity programs, as they were accomplished in Brownian elution mode [27]. The flow-rate gradients presented in this work result in changes of the retention ratios. Thus, they are tools for force-field programming.

2. Experimental

The experimental equipment has been described previously [19]. The separation channel was cut in a spacer of 80 μm height. The spacer was then sandwiched between two float glass plates and the latter were clamped together with two Plexiglas bars. The width, length, and geometrical void volume of the channel (including inlet and outlet apices) were 2 cm, 35 cm, and 0.51 ml, respectively. Flow-rate programming was performed with a HP 1100 Series Quaternary Pump (Hewlett-Packard). A UVM 4 spectrophotometric detector (Development Workshops AS CR, Prague, Czech Republic), equipped with a Z-shaped cell with an optical path of 5 mm, was operated at 254 nm. Fractograms were recorded with elution time as X-axis and converted to elution volume as X-axis.

Milli-Q water was applied as the carrier liquid. The model mixture consisted of non-porous silica gel particles of diameter 1.6 μm (a gift from Prof. E.

Kováts, SFIT, Lausanne, Switzerland) and porous particles (Sepharon SGX) of nominal diameters 5 and 10 μm (Tessek, Prague, Czech Republic). They were prepared as follows: 8 mg/ml suspensions of analytes 1 (porous 10 μm silica) and 2 (porous 5 μm silica) were sonicated for 10 min. Ultrasound stirring was followed by boiling for 3 min in order to remove gas from the pores and to thoroughly wet all the particle cavities. A 2 mg/ml suspension of analyte 3 (non-porous 1.6 μm silica) was sonicated for 10 min. Equal volumes of suspensions 1, 2, and 3 (treated as described above) were mixed and recurrently sonicated before each injection for 2 min. A 2 μl volume of the model mixture was injected. The stop-flow time was 60 s. The same mixture was used for all the measurements reported in this work.

3. Results and discussion

The major challenge of this work was to show that flow-rate programming in GFFF could provide better resolution than any constant flow-rate with simultaneous time reduction. With this goal in mind, we had to deal with some complications. The model mixture is not ideal. It contains two analytes with a broad overlapping size distribution (analytes 1 and 2). This polydispersity results in wide and seriously overlapping peaks 1 and 2 [9] and obscures the intrinsic sharpness produced by the tested flow-rate gradients. The second complication is caused by the unequal number of particular particles per volume unit of the model mixture: there are $1.02 \cdot 10^7$ particles of analyte 1 ($d = 10$ μm), $8.15 \cdot 10^7$ particles of analyte 2 ($d = 5$ μm), and $4.24 \cdot 10^8$ particles of analyte 3 ($d = 1.6$ μm) in 1 ml of the model suspension. Furthermore, particles of different size show different light dispersion. Due to the particle size-based response of the UV detector and the unequal concentrations in the model mixture, each particular peak in the fractogram shows a different height and different area compared to the others.

The third problem is to define an appropriate parameter for evaluation of the optimization effect of the tested flow-rate gradients. The peaks are not Gaussian, which disqualifies the generally used calculation of peak resolution for the case when the peaks are not baseline separated. Thus, it is reasonable to define a parameter that would enable comparisons of the gradient separations in our non-standard situation. We arbitrarily defined parameters $R^*_{1,2}$ and $R^*_{2,3}$ by the equations presented in Table 1. Using these parameters, we compared all the separations yielding $R^*_{1,2} > 1$ (Table 1). In the following, the separations yielding $R^*_{1,2} < 1$ are described as non-successful. Despite the above-mentioned complications, the aim of this work was achieved, as described below.

3.1. Constant flow-rate

The suitable range of flow-rates for force-field programming was determined in previous work [19]. For a channel height of 80 μm, the properly functioning flow-rates were in the range 0.2–1.3 ml/min. Fig. 1 presents fractograms of the model mixture obtained at three constant flow-rates within this

Table 1
Comparison of the effects of selected flow-rate gradients on separation of the model mixture. The parameters $R^*_{1,2}$ and $R^*_{2,3}$ are arbitrarily defined as follows:

$$R^*_{1,2} = \frac{b-a}{\alpha+\beta}$$

where a is the elution time (volume) of peak 1, b is the elution time (volume) of peak 2, α is the tailing half-width of peak 1 taken at one-half of its height and β is the fronting half-width of peak 2 taken at one-half of its height;

$$R^*_{2,3} = \frac{c-b}{\gamma+\delta}$$

where b is the elution time (volume) of peak 2, c is the elution time (volume) of peak 3, γ is the tailing half-width of peak 2 taken at one-half of its height and δ is the fronting half-width of peak 3 taken at one-half of its height

Elution conditions	Elution time as the X-axis		Elution volume as the X-axis		Total separation time (min)
	$R^*_{1,2}$	$R^*_{2,3}$	$R^*_{1,2}$	$R^*_{2,3}$	
Gradient B	1.1	3.9	1.1	3.9	4.5
Gradient D	1.2	4.0	1.2	4.1	4.1
Gradient F	1.9	5.7	1.9	5.8	4.2
Gradient H	1.4	3.8	1.4	3.8	6.8
Gradient I	1.4	3.7	1.4	3.7	5.3
Gradient J	1.6	3.7	1.6	3.7	4.0
Constant flow-rate 0.2 ml/min	1.4	4.3	1.4	4.3	19

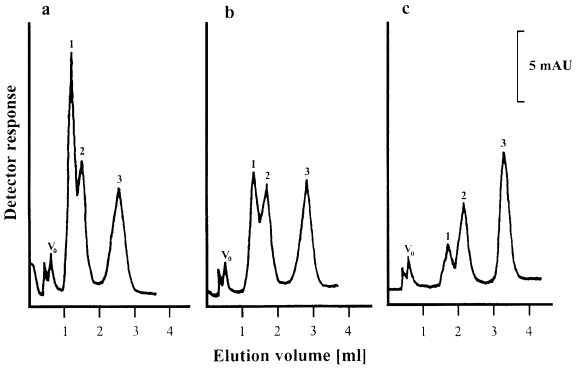

Fig. 1. Fractograms of the model silica mixture at three constant flow-rates: (a) 1.0 ml/min, (b) 0.5 ml/min and (c) 0.2 ml/min. V_0 denotes the peak corresponding to the void volume and peaks 1, 2, and 3 refer to analytes 1 (10 μm), 2 (5 μm), and 3 (1.6 μm), respectively. Based on the arbitrarily defined parameter $R^*_{1,2}$, the separations were evaluated as follows: (a) non-successful, (b) non-successful, (c) $R^*_{1,2} = 1.4$, $R^*_{2,3} = 4.3$.

range. It is clear that, with increasing flow-rate, the retention time difference between peaks 1 and 2 decreases, which affects their resolution. The best resolution was obtained at a flow-rate of 0.2 ml/min ($R^*_{1,2} = 1.4$), however the total separation time was 19 min. At flow-rates of 0.5 and 1 ml/min, the speed of separation was increased at the expense of the resolution. Based on the parameter $R^*_{1,2}$, these separations were evaluated as being non-successful. The total separation times were 6.4 and 3 min.

At a flow-rate of 0.2 ml/min, the differences in the heights and areas of peaks 1, 2 and 3 are probably caused by the particle size-based response of the UV detector, by the unequal numbers of particular particles per 1 ml of the model mixture, and by the separation mechanism of the focusing elution mode induced by HLF. At different flow-rates, the ratio of peak heights differs. The lowest peak 1 at a flow-rate of 0.2 ml/min (Fig. 1c) becomes about equal when the flow-rate increases to 0.5 ml/min (Fig. 1b) and develops into the highest at a flow-rate of 1 ml/min (Fig. 1a). This is due to the increasing magnitude of HLF and thus the enhanced focusing and elevating effect of increasing flow-rate [23–26]. As HLF act strongly on larger particles, the largest 10 μm particles of analyte 1 are elevated and focused most with increasing flow-rate and thus the height of peak 1 increases dramatically.

Fig. 2 shows the effects of focusing and band broadening depending on flow-rate. In general, the focusing effect is provided by HLF action (opposing gravity). Increasing flow-rates lead to the formation of narrower zones located at longer distances from the channel bottom. A narrower zone is less dispersed by the non-uniform flow profile of the carrier liquid than a broader zone. Moreover, band broadening is also related to the position of the focused zone

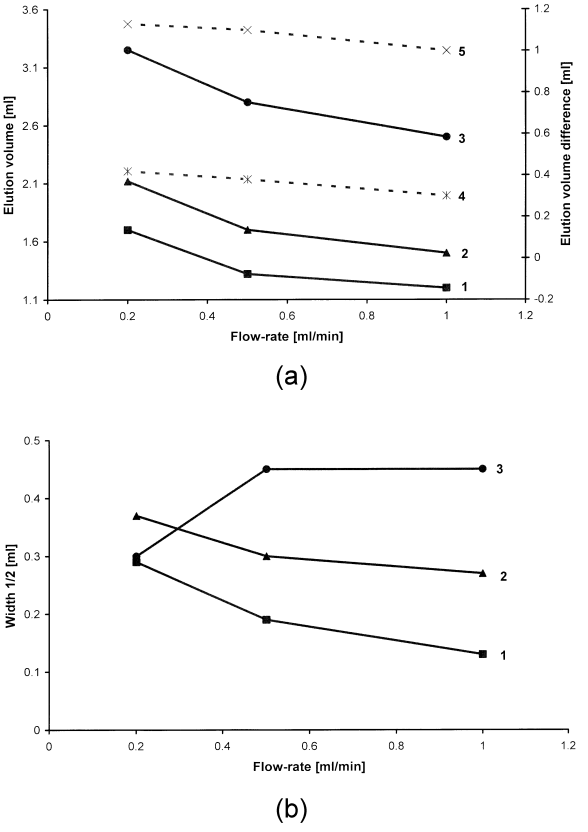

Fig. 2. (a) Dependence of the elution volume of particular peaks and the elution volume difference between the peaks on the flow-rate. The values of elution volume were obtained from the fractograms in Fig. 1. Curves 1, 2, and 3 show the elution volumes of peaks 1, 2, and 3, respectively. Curve 4 expresses the elution volume difference between peaks 1 and 2. Curve 5 expresses the elution volume difference between peaks 2 and 3. (b) Dependence of peak width on the flow-rate. The values of the peak width were obtained from fractograms of separately injected particular analytes fractionated under the same conditions as for Fig. 1. The width of each peak (denoted Width 1/2) was taken at one-half of its height from the elution volume *X*-axis record. Curves 1, 2, and 3 refer to peaks 1, 2, and 3, respectively. Each data point is the average of five measurements with a relative standard deviation of <2% for most points and never exceeding 5%.

inside the channel. The zone located at a higher position is less dispersed than the zone near the channel bottom because of the shallower flow-rate gradient at the higher positions [29,30].

Fig. 2a demonstrates the dependence of the elution volume of particular peaks (obtained from Fig. 1) on the flow-rate. It shows that the elution volume difference between peaks 1 and 2 decreases slightly with increasing flow-rate (curve 4). This affects the peak resolution. In order to investigate the dependence of the peak width on the flow-rate, we evaluated the fractograms of separately injected particular analytes. The widths of the peaks taken at one-half of their heights are plotted against flow-rate in Fig. 2b. It is clear that, within this flow-rate range, peaks 1 and 2 tend to narrow with increasing flow-rate (due to the enhanced focusing and elevating effect of HLF), which should contribute to improvement of their resolution. Based on the combination of the two counteracting effects reported in Fig. 2a and b, the optimal flow-rate gradient was determined which would provide reasonable resolution of peaks 1 and 2 and complete separation of peaks 2 and 3 with a short separation time.

3.2. Linear flow-rate gradients

Several linear flow-rate gradients with different slope were tested. For all the gradients presented in Fig. 3 the flow-rate was started at 0.5 ml/min. The flow-rate was then increased up to 1 ml/min within 5 min with gradient A, within 4 min with gradient B and within 3 min with gradient C, as shown by the plots of the flow-rate programs in Fig. 3. It is clear that no significant benefit was obtained with the tested linear flow-rate gradients. Among these programs, the best result was achieved by gradient B. The value of parameter $R^{*}_{1,2}$ was 1.1 and the total separation time was 4.5 min. The baseline is drifting down, which is caused by the gradually increasing flow-rate.

3.3. Multilinear flow-rate gradients

The two selected multilinear gradients shown in Fig. 4 were started at 0.5 ml/min and increased to 0.76 ml/min within 2.1 min, which is the same slope as that of gradient B. This first part was followed by a steeper slope reaching the terminal value of 1.26 ml/min within 2 min with gradient D (the slope increased twice) and 1 min with gradient E (the slope increased four times). The run was then completed at this terminal value. Gradient D provided the best result ($R^{*}_{1,2} = 1.2$) of all the linear and multilinear gradients. The total separation time was 4.1 min, and $R^{*}_{2,3}$ was 4.0. The baseline drifted down proportion-

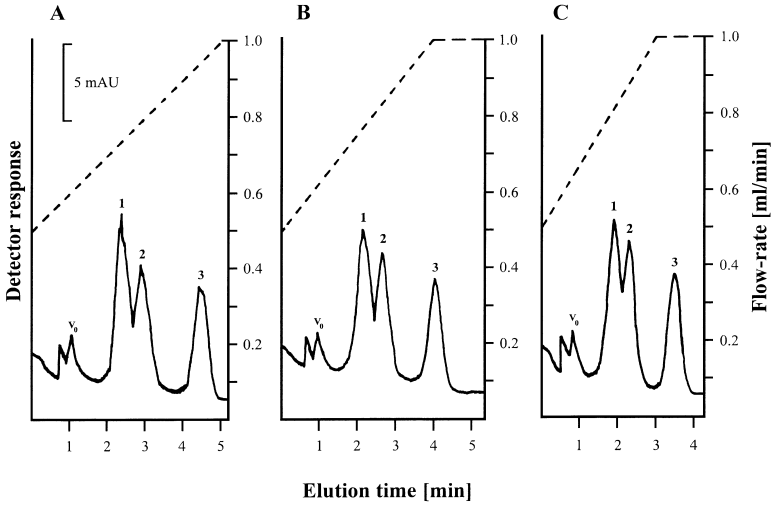

Fig. 3. Fractograms of the model silica mixture obtained under conditions of linear flow-rate gradients A, B and C. The flow-rate programs are described by the dashed line plots. Symbols V_0, 1, 2, and 3 and the evaluation are as described in Fig. 1: (A) non-successful, (B) $R^{*}_{1,2} = 1.1$, $R^{*}_{2,3} = 3.9$, (C) non-successful.

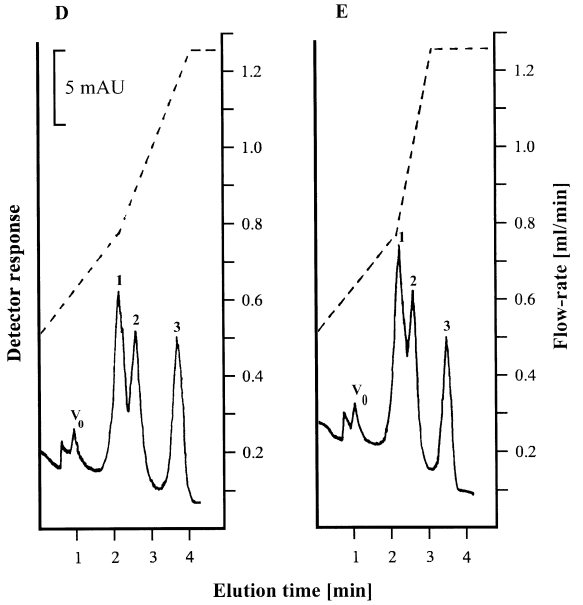

Fig. 4. Fractograms of the model silica mixture obtained under conditions of multilinear flow-rate gradients D and E. The flow-rate programs are described by the dashed line plots. Symbols V_0, 1, 2, and 3 and the evaluation are as described in Fig. 1: (D) $R^*_{1,2} = 1.2$, $R^*_{2,3} = 4.0$, (E) non-successful.

ally to the increasing flow-rate. Gradients D and E provide sharper peaks than gradients A, B, and C. One has to consider that, during multilinear gradients, starting from the separation time of 2.1 min, the velocity gradient of the zone passing through the detector is much steeper. Thus, as the last half of each peak with gradients D and E is swept out of the channel much more rapidly than the first half, the peaks look sharper. The parameter $R^*_{1,2}$ suggests that no substantial optimizing effect was achieved by multilinear flow-rate gradients.

3.4. Parabolic flow-rate gradients

We tested two types of parabolic gradients: flow-rate increasing in proportion to the square of time (gradient F, see Eq. (1)) and to the square root of time (gradient G, see Eq. (2)) according to the following functions:

$$v = 0.5 + 0.048 \cdot t^2 \quad (1)$$

$$v = 0.5 + 0.408 \cdot t^{1/2} \quad (2)$$

where v is the flow-rate (ml/min) and t is time (min). With gradient F this increase continued until a terminal flow-rate value of 1.32 ml/min and the run was then completed at this value. With gradient G the fractionation was finished when the program reached a flow-rate value of 1.26 ml/min. The flow-rate programs are expressed by the plots in Fig. 5. Under the conditions of gradient G, the separation was finished in 3.1 min. However, based on the parameter $R^*_{1,2}$, the separation was evaluated as being non-successful. On the contrary, gradient F improved both $R^*_{1,2}$ and $R^*_{2,3}$. The obtained value of $R^*_{1,2}$ was 1.9 and $R^*_{2,3}$ was 5.7, which were the best $R^*_{1,2}$ and $R^*_{2,3}$ values of all the tested flow-rate programs. The total separation time was 4.2 min. The values of $R^*_{1,2}$ and $R^*_{2,3}$ were improved even compared to the lowest constant flow-rate ($R^*_{1,2} = 1.4$ and $R^*_{2,3} = 4.3$ at a flow-rate of 0.2 ml/min). In order to draw conclusions about the true peak sharpness and symmetry, we also converted the fractograms into volume-scaled co-ordinates. In Fig. 6 the elution time X-axis

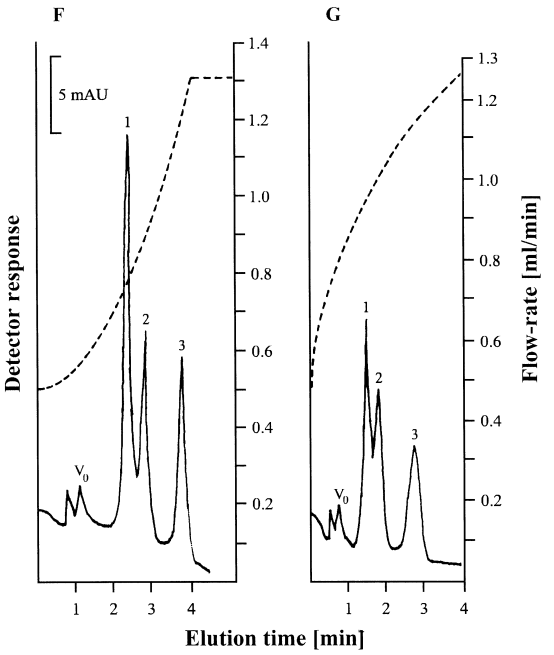

Fig. 5. Fractograms of the model silica mixture obtained under the conditions of parabolic flow-rate gradients F and G. The flow-rate programs are described by the dashed line plots. Symbols V_0, 1, 2, and 3 and the evaluation are as described in Fig. 1: (F) $R^*_{1,2} = 1.9$, $R^*_{2,3} = 5.7$, (G) non-successful.

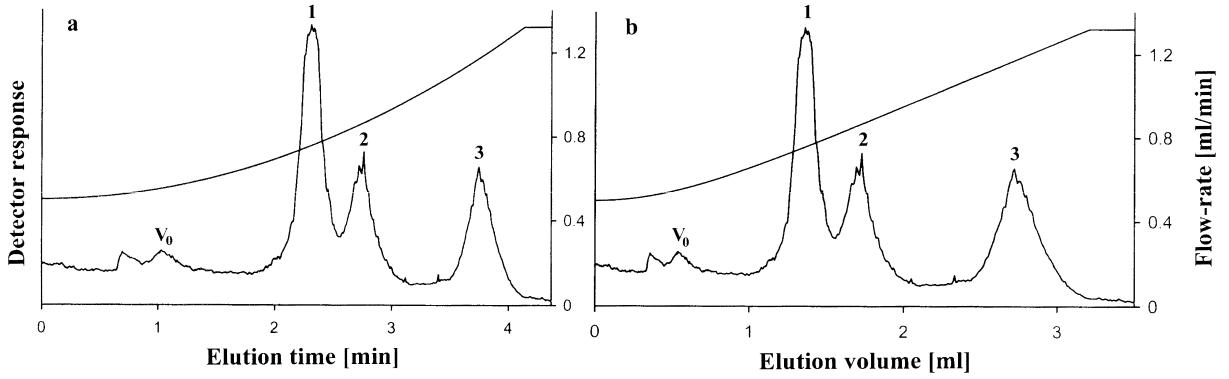

Fig. 6. Comparison between elution time *X*-axis (a) and elution volume *X*-axis (b) plots of the most successful flow-rate gradient (gradient F). The fractogram was recorded with elution time as *X*-axis and converted to elution volume as *X*-axis. The flow-rate program is described by the full line plots. Symbols V_0, 1, 2, and 3 and the evaluation are as described in Fig. 1. The values of $R^*_{1,2}$ and $R^*_{2,3}$ are presented in Table 1.

record of gradient F is converted to the elution volume *X*-axis record. It can be seen that this conversion did not affect the value of $R^*_{1,2}$ and even improved the value of $R^*_{2,3}$ to 5.8 (values are presented in Table 1).

The advantage of the parabolic flow-rate program for this particle mixture is illustrated by a comparison between the multilinear gradient D and the parabolic gradient F. Both gradients started at 0.5 ml/min and increased to about 1.3 ml/min in about 4 min. The only difference is in the shape of the flow-rate plots. It seems that the unique separation capability of the parabolic gradient is given by the mild starting slope of the flow-rate plot, which gradually steepens. We can conclude that this is a very successful flow-rate program. The demand for expensive equipment (a programmable pump) and the disadvantage of the drifting baseline evoked further effort.

3.5. Step gradients

Several step gradients were suggested to combine the benefits of both low and high flow-rate in a technically simple way. The effect of starting flow-rate is demonstrated in Fig. 7. The lengths of the low flow-rate periods at different starting flow-rates were settled in order to set the high flow-rate when the void volume peak had just passed through the detector (4 min at 0.2 ml/min with gradient H, 3 min at 0.3 ml/min with gradient I, 1.6 min at 0.5 ml/min with gradient J). One practical advantage is related to a long and low starting flow-rate: it enables settlement of yet non-relaxed particles and thus reduction of the stop-flow time [31]. In order to demonstrate this benefit in a previous work, an intentionally incorrect stop-flow time (30 s) was used with gradient J (starting at 0.5 ml/min for 1.6 min) [31]. With a stop-flow time of only 30 s, the double-topped peak 3 showed unfinished sedimentation of the smallest particles. However, under the conditions of a longer low flow-rate period and lower starting flow-rate (4 min at 0.2 ml/min), the same stop-flow time of only 30 s was satisfactory and the perfectly pronounced peak 3 confirmed thorough settlement of the smallest particles [31]. This shows that we can combine a long and low starting flow-rate period with a shorter stop-flow time than calculated, which can be useful in some cases. The effect of the duration of the low flow-rate period on the proportional heights of peaks 1 and 2 has also been demonstrated [31].

At step gradients H, I, and J, the resolution of peaks 1 and 2 is maintained or improved compared to a constant flow-rate of 0.2 ml/min and peak 3 is baseline separated from peak 2. The total separation times and the values of $R^*_{1,2}$ are as follows: 6.8 min and 1.4 with gradient H, 5.3 min and 1.4 with gradient I, and 4 min and 1.6 with gradient J.

It follows that, with stepped program J, the value of $R^*_{1,2}$ is improved compared to the flow-rate of 0.2 ml/min, and the total separation time is very satis-

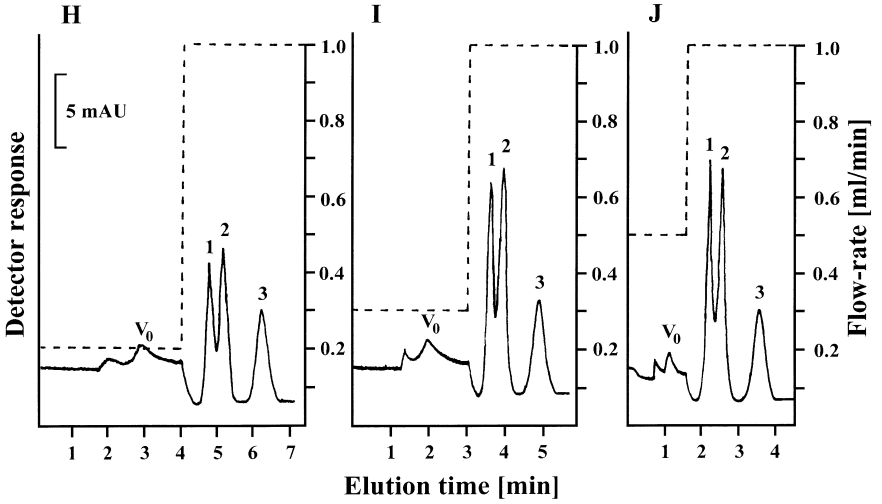

Fig. 7. Fractograms of the model silica mixture obtained under the conditions of step flow-rate gradients H, I and J. The flow-rate programs are described by the dashed line plots. Symbols V_0, 1, 2, and 3 and the evaluation are as described in Fig. 1: (H) $R^*_{1,2} = 1.4$, $R^*_{2,3} = 3.8$, (I) $R^*_{1,2} = 1.4$, $R^*_{2,3} = 3.7$, (J) $R^*_{1,2} = 1.6$, $R^*_{2,3} = 3.7$.

factory. Moreover, the stepped programs avoid the problems with drifting baseline. We only obtain a drop on a constant baseline. The benefit of the technical simplicity also has to be taken into account.

3.6. Overloading effect

The influence of increasing amounts of injected particles on separation in GFFF has been investigated previously [32]. In this work, we demonstrated the overloading effect under the conditions of a programmed flow-rate. Step gradient H was accomplished with different increasing amounts of the model mixture. The following sample volumes were injected: 2, 3, 4, 6 and 8 μl. Based on the previously discussed mechanism of the overloading effect [32], one can anticipate that an increase of the injected sample amount would seriously interfere with the resolution of peaks 1 and 2. Fig. 8 bears out this assumption and reveals that an undue decrease of $R^*_{1,2}$ occurred when the injected volume exceeded 4 μl. Further increase of the injected amount resulted in a deterioration of the separation. The shape and retention time changes of peak 3 in Fig. 8a–e show the manifestation of the overloading effect as described in Ref. [32]. When applying flow-rate gradients, one has to pay attention to the optimization of the amount injected.

4. Conclusion

The major challenge of this work was to find a flow-rate gradient that would provide improved resolution of the first two peaks and the complete resolution of the last two peaks of the sample with a reduced separation time. In general, the flow-rate gradients yielded reduced separation times. However, some of them resulted in poorer resolution of the first two peaks. Moreover, the gradually increasing flow-rate produced problems with the baseline drifting down.

Several of the tested flow-rate gradients satisfy the above-mentioned requirements. The best resolution was achieved with the convex parabolic gradient. However, the demand for a programmable pump makes it rather less accessible. Very satisfactory resolution with a slightly shorter separation time was provided by step gradient J, which could be generated by common equipment. Whereas with linear and parabolic gradients the baseline drifts down proportionally to the increasing flow-rate, step gradients only produce a drop on a straight baseline.

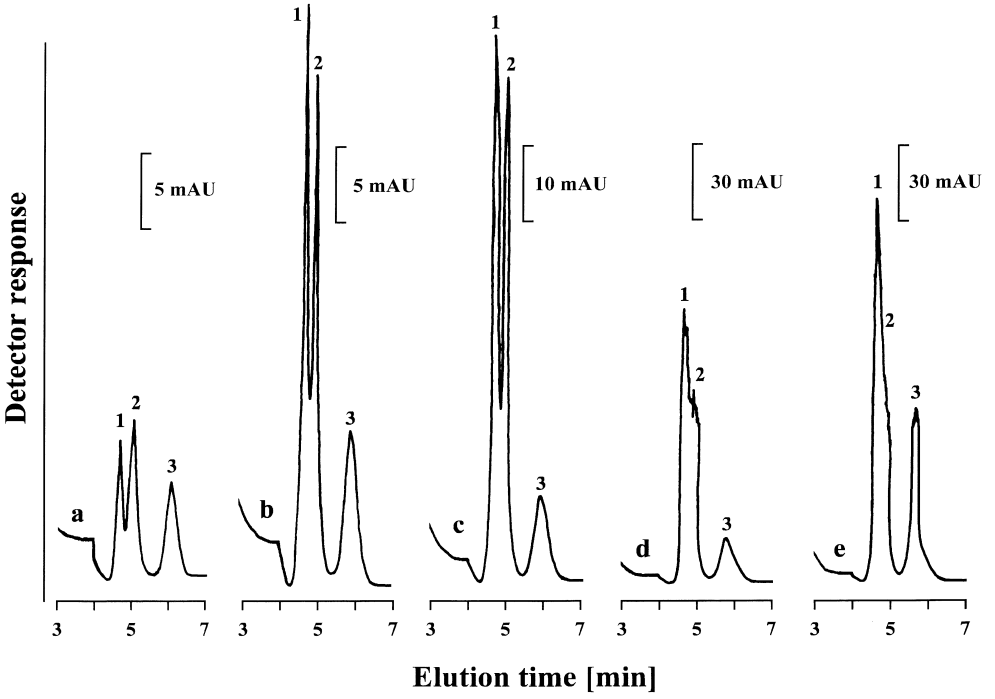

Fig. 8. The influence of increasing injected volume of the model silica mixture (overloading effect) on fractionation under the conditions of step gradient H. The volumes of the model mixture injected were (a) 2 μl, (b) 3 μl, (c) 4 μl, (d) 6 μl, (e) 8 μl. The onset of a flow-rate of 1 ml/min is indicated by the drop on the baseline in each fractogram. Peaks 1, 2, and 3 refer to analytes 1 (10 μm), 2 (5 μm), and 3 (1.6 μm), respectively.

Acknowledgements

This work was supported by grant No. A4031805/1998 from the Grant Agency of the Academy of Sciences of the Czech Republic. František Matulík is gratefully appreciated for technical support and Josef Chmelík Jr. for introductory programming of the flow-rate gradients.

References

[1] J.C. Giddings, Sep. Sci. 1 (1966) 123.
[2] J.C. Giddings, M.N. Myers, Sep. Sci. Technol. 13 (1978) 637.
[3] K.D. Caldwell, T.T. Nguyen, J.C. Giddings, M.N. Myers, Sep. Sci. Technol. 14 (1979) 935.
[4] J. Pazourek, K.-G. Wahlund, J. Chmelík, J. Microcol. Sep. 8 (1996) 331.
[5] P.J.P. Cardot, J. Gerota, M. Martin, J. Chromatogr. 568 (1991) 93.
[6] E. Urbánková, A. Vacek, J. Chmelík, J. Chromatogr. B 687 (1996) 449.
[7] J. Chmelík, A. Krumlová, J. Čáslavský, Chem. Pap. 52 (1998) 360.
[8] J.C. Giddings, M.N. Myers, K.D. Caldwell, J.W. Pav, J. Chromatogr. 185 (1979) 261.
[9] J. Pazourek, E. Urbánková, J. Chmelík, J. Chromatogr. A 660 (1994) 113.
[10] J. Pazourek, J. Chmelík, J. Microcol. Sep. 9 (1997) 611.
[11] R.E. Peterson II, M.N. Myers, J.C. Giddings, Sep. Sci. Technol. 19 (1984) 307.
[12] J. Pazourek, J. Chmelík, Chromatographia 35 (1993) 591.
[13] H. Meng, K.D. Caldwell, J.C. Giddings, Fuel Proc. Technol. 8 (1984) 313.
[14] J.C. Giddings, V. Kumar, P.S. Williams, M.N. Myers, in: C.D. Craver, T. Provder (Eds.), Polymer Characterization: Physical Property, Spectroscopic, and Chromatographic Methods, ACS Advances in Chemistry Series, Vol. 227, American Chemical Society, Washington, DC, 1990, Chapter 1.
[15] P.S. Williams, J.C. Giddings, R. Beckett, J. Liq. Chromatogr. 10 (1987) 1961.
[16] P.S. Williams, J.C. Giddings, Anal. Chem. 59 (1987) 2038.
[17] S.K. Ratanathanawongs, J.C. Giddings, Anal. Chem. 64 (1992) 6.
[18] J. Chmelík, J. Chromatogr. A 845 (1999) 285.
[19] J. Plocková, J. Chmelík, J. Chromatogr. A 868 (2000) 217.
[20] J.C. Giddings, Sep. Sci. Technol. 18 (1983) 765.

[21] J. Janča, J. Chmelík, Anal. Chem. 56 (1984) 2481.
[22] R.G. Cox, H. Brenner, Chem. Eng. Sci. 23 (1968) 147.
[23] H. Brenner, Adv. Chem. Eng. 4 (1966) 287.
[24] B.P. Ho, L.G. Leal, J. Fluid Mech. 65 (1974) 365.
[25] V.L. Kononenko, J.K. Shimkus, J. Chromatogr. 520 (1990) 271.
[26] P.S. Williams, T. Koch, J.C. Giddings, Chem. Eng. Commun. 111 (1992) 121.
[27] J.C. Giddings, K.D. Caldwell, J.F. Moellmer, T.H. Dickinson, M.N. Myers, M. Martin, Anal. Chem. 51 (1979) 30.
[28] F.J.F. Yang, M.N. Myers, J.C. Giddings, Anal. Chem. 46 (1974) 1924.
[29] J.C. Giddings, Sep. Sci. Technol. 18 (1983) 765.
[30] J. Janča, J. Chmelík, Anal. Chem. 56 (1984) 2481.
[31] J. Plocková, J. Chmelík Jr., F. Matulík, J. Chmelík, Poster No. 10, in: Presented at the 8th International Symposium on Field-Flow Fractionation, Paris, 6–8 September, 1999.
[32] J. Pazourek, J. Chmelík, J. Chromatogr. A 715 (1995) 259.